

LIVE LOAD TEST OF A 54-YEAR OLD PRESTRESSED CONCRETE VOIDED SLAB BRIDGE

Bernard L. Kassner, Ph.D., P.E., Virginia Center for Transportation Innovation and Research, Charlottesville, VA

Soundar S.G. Balakumaran, Ph.D., Virginia Center for Transportation Innovation and Research, Charlottesville, VA

ABSTRACT

Bridge superstructures built with adjacent, prestressed concrete voided slabs are a common alternative for bridge owners because of their low profiles, lack of need for deck formwork, faster construction times, and consequently, low worker accident rates. However, the mechanism for transferring shear between the beams often fails, leading to leakage of salt-laden runoff water between the individual beams and increased corrosion of prestressing strands, thus resulting in a shortened lifespan. Researchers had the opportunity to conduct a limited live load test on an adjacent, prestressed concrete voided slab structure that had been in service for 54 years. Two beams were of particular concern due to obvious holes in the bottom exposing corroded prestressing reinforcement. The load test measured longitudinal strain at mid-span and the quarter-spans, horizontal and vertical differential displacement between adjacent members, and rotations at the beam ends. Overall, the results showed that the bridge was in good structural condition. Strains were relatively small, with the supports being stiffer than expected and the bottom of beams in compression under the heaviest load tested. Girder distribution factors were slightly better than assumed in the AASHTO design specifications, and the shear keys performed well with minimal relative displacements between adjacent members.

Keywords: Prestressed, Concrete, Adjacent, Slab, Shear key, Load test

INTRODUCTION

Voided adjacent slab bridges are built by placing narrow prestressed slabs side by side and connecting them with longitudinal shear keys and transverse post-tensioning ties such that the individual slabs act monolithically. The slabs typically contain voids to reduce the self-weight of the superstructure. The top of the voided slabs typically act as the deck for vehicular traffic, thus eliminating the costs and time involved with formwork for the deck. In some cases, however, a wearing surface may be applied. Nevertheless, the rapid construction time also helps to minimize interruption to traffic in cases of total bridge or superstructure replacement projects. Voided slabs also have a much shallower profile relative to bridges composed of AASHTO prestressed concrete or steel girders with concrete decks of similar span. Therefore, these bridges may provide greater vertical clearance for vehicular traffic or hydraulic flow underneath the bridge¹. Furthermore, the continuous (flat) bottom of the superstructure also helps to prevent debris from being caught underneath the bridge during high-water events, thus avoiding blockage of the stream flow and the need for maintenance crews to clear obstructions after the water has subsided. Fig. 1 shows a partial section view of a voided slab superstructure. Note that these types of structures often have some type of wearing surface placed on top of the beams, and that wearing surface is usually asphalt. In Virginia, however, bridges on routes that exceed an average daily traffic (ADT) of 4,000 vehicles are required to have a concrete deck, as prescribed in Table 1. Also, the number of transverse post-tensioned tendons can vary depending on the depth and span of the beams.

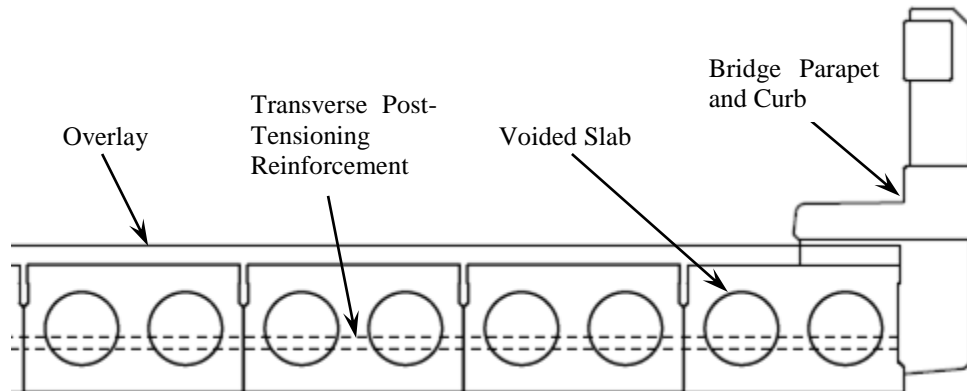


Fig. 1 Partial cross-section of a voided slab structure.

Table 1 Standard overlays for a given average daily traffic (ADT) and average daily truck traffic (ADTT) on Box Girders.

Design Year ADT	ADTT	Deck Overlay
≤ 4000	≤ 100	Asphalt Overlay
> 4000	100 < ADTT ≤ 200	5-in. concrete deck with single layer of reinforcement
> 4000	> 200	7.5-in. concrete deck with two layers of reinforcement

There are certain disadvantages with this type of bridge, which can detract from the aforementioned advantages. In particular, if the longitudinal shear keys fail, the joints begin

to leak, as is reported to occur frequently in service. Runoff water from the deck carrying deicing salts then diffuses to the sides and bottom of the voided slabs, where the concrete cover is shallower compared to the top of the members. The shallower cover provides less resistance to penetration of salt contaminants through the concrete to the steel and results in a shorter time before corrosion begins to deteriorate the longitudinal prestressing reinforcement. This prestressing reinforcement is the primary tension-carrying components of the prestressed composite beams. Moreover, post-tensioning ties start corroding with the failure of shear keys. Such deterioration can significantly reduce the load-carrying capacity of the structure and can pose a safety problem for the traffic over time.

As of June 2014, the Virginia Department of Transportation (VDOT) had 320 adjacent, prestressed concrete slab bridges, which was roughly 2.5% of the bridge inventory. Out of those 320 bridges, about 7% had a superstructure rating of 4 or 5, meaning fair to poor condition based on NBI visual inspection and engineering analysis.

The Adkins Road Bridge was one such structure. Constructed in 1959, this five-span, voided slab structure had a 7° horizontal curve with a 5.5° superelevation. In order to accommodate this curve, the bent caps had a slight wedge shape in plan, where the downstream side of the cap was slightly wider than the upstream end [See Fig. 2(a)]. The joints between the cap and the voided slabs were filled with a pourable sealant, as shown in Fig. 2(b). Each adjacent, prestressed concrete slab was 21 in. high and 3 ft wide, with an overall bridge width of 29.1 ft from edge to edge of the exterior beams. The spans were either 40.75 ft or 41.5 ft long, with an overall length of 207.5 ft along the circular curve. See Fig. 3 for an overall plan of the bridge. The individual slabs were tied together transversely using 1¼-in. diameter, plain structural rod that was tensioned to 30 kips, and the detail used to transmit shear between beams is shown in Fig. 4. Note that there was widespread efflorescence on the bottom of the structure due to water leakage, as seen in Fig. 5. This leakage indicated the ineffectiveness of the longitudinal joints, as is typical for this type of construction. Unfortunately, the condition of the tie rods could not be ascertained. Limited past experience had found that such transverse reinforcement in older structures like the Adkins Road bridge either had 100% section loss or were otherwise severely corroded. Thus, the assumption going into the testing was that the transverse reinforcement provided little beneficial effect.

Span 3 of the Adkins Road Bridge was the most problematic in that two beams had large spalls with exposed prestressing strands, neither of which had been previously reported. The spall in Beam 5 was actually an 8 in. x 1 ft hole in the bottom of the slab at the quarter-point closest to Bent 2, shown in Fig. 6. The hole showed poor consolidation around the reinforcement and the Sonotube form used to create the voids in the slab. The reinforcement was relatively clean of rust, although one of the strands had a broken wire. The 5 ft by 2.5 ft spall in Beam 4 was located at the quarter-span nearest to Bent 3 in Span 3. Again, there was evidence of poor consolidation, although the reinforcement was heavily corroded, as shown in Fig. 7. According to the district bridge engineer, a bridge safety inspector heard a loud noise while inspecting one of these two locations. At that point, the district bridge engineer immediately closed the structure to traffic and asked for a load test.

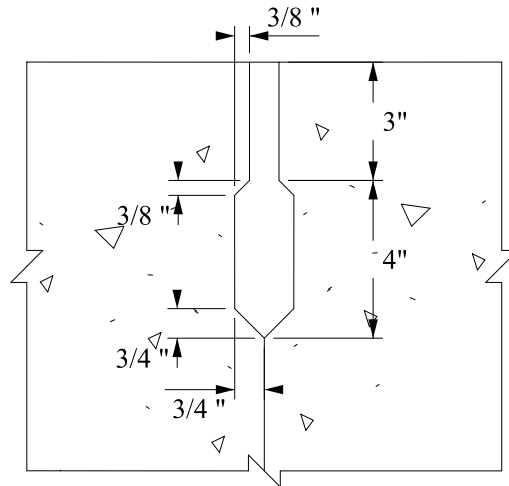


Fig. 4 Shear key detail for the Adkins Road bridge.



Fig. 5 Efflorescence on the bottom of and along the longitudinal joints of the voided slabs



Fig. 6 Poorly consolidated concrete in Beam 5, near the quarter-point closest to Bent 2, Span 3.



Fig. 7 Poorly consolidated concrete below corroded strands in Beam 4, near the quarter-point closest to Bent 3, Span 3.

TESTING

INSTRUMENTATION

Instrumentation for this load test consisted of strain transducers, linear variable differential transformers (LDVTs), and tiltmeters. With the exception of the deflectometers, all of the instruments were manufactured by Bridge Diagnostics, Inc. (BDI). Fig. 8 shows the locations of the various instruments used during the load test.

The strain gauges were reusable, surface-mounted BDI ST350 Intelligent strain transducers, which had a 3-inch gauge length and an accuracy of $\pm 2\%$ with a strain range of $\pm 2,000 \mu\epsilon$. All ST350 gauges placed on the girders were located at mid-width of the bottom of the beams. The strain gauges placed at mid-span were designed to capture the maximum strain in the concrete, while the strain gauges placed at the quarter-spans in Beams 3 and 4 served two purposes. The first was to compare strains between the two quarter-points for each beam. The second was to compare strains in adjacent beams at the quarter-span closer to Bent 3, where Beam 4 had exposed prestressing strands. While no soundings (that is, chain drag or hammer survey) were conducted prior to load testing, there were no visible cracks or spalls on Beam 3 at this location.

Although the barrier rails were constructed of cast-in-place concrete, the researchers applied the same type of BDI strain transducers without gauge extensions in an attempt to assess the stiffness provided by the barrier rails. The two gauges placed on the upstream barrier were located on the top of the curb and the bottom of the face of the top rail, respectively. All of the strain gauges were attached using rapid-setting adhesive applied to the concrete surface.

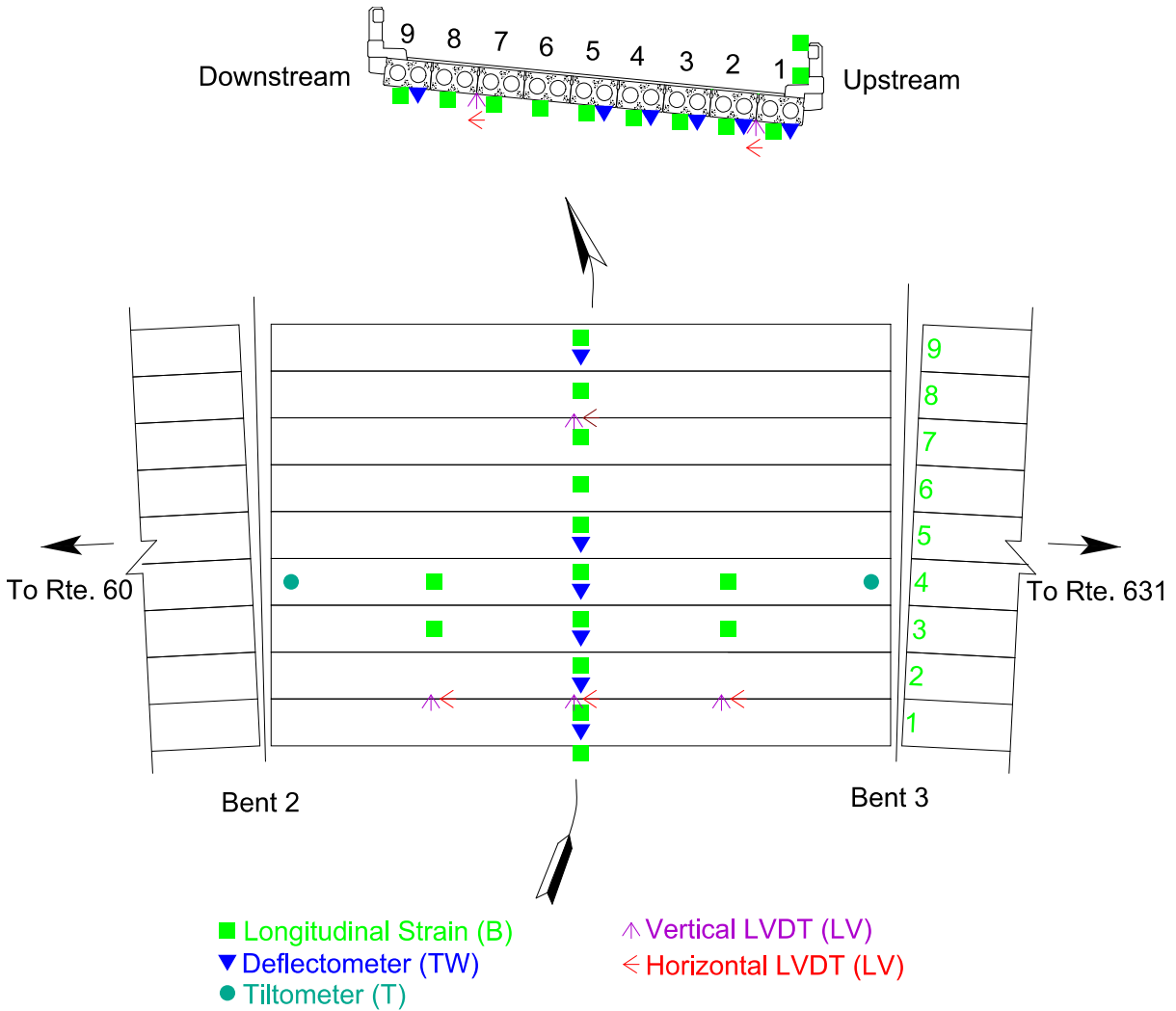


Fig. 8 Instrumentation plan for the live load test of Span 3 of the Adkins Road bridge.

Linear Variable Differential Transformers

Eight LVDTs were set up to measure both vertical and horizontal differential movement between two sets of adjacent voided slabs. Each LVDT had a range of ± 1 inch with a maximum linearity error of $\pm 0.5\%$ of full scale. All plungers were set approximately at the middle of the displacement range. The LVDT locations at mid-span were selected for two reasons. The first was to compare movement in a longitudinal joint adjacent to an exterior girder, Joint 1 between Beams 1 and 2, to movement in a longitudinal joint for a pair of interior girders, Joint 7 between Beams 7 and 8. The second was to contrast a joint in relatively poor condition (on the upstream side of the bridge) with a joint that appeared to be in relatively good condition (closer to the downstream side of the bridge). The remaining LVDTs were placed at the quarter-points of Joint 1, as a comparison of differential movements between those two points of the span and the mid-span.

Tiltmeters

The last type of sensor installed on the bridge was a tiltmeter, which measured the rotation of Beam 4 near the bents. Two devices were located as close as practical to the opposite ends of the beam. The tiltmeters had a range of -10° to $+10^{\circ}$ and an accuracy of 2% of full scale.

Data Acquisition

All instruments were hard-wired to one of BDI's STS-Wi-Fi nodes attached to the underside of the bridge. The nodes then wirelessly transmitted the information to the STS-Wi-Fi Mobile Base Station, which was then relayed wirelessly to a laptop computer, where the data was stored for post-processing. Each instrument was sampled and recorded at a rate of 25 Hz. The BDI system also included a laser-based counter that was attached to the wheel well of the truck in order to track the speed and longitudinal location of the truck throughout a given load test.

LOAD TRUCKS

Typical VDOT dump trucks served as the live load traveling across the bridge. Note that there were three separate dump trucks used for the tests, each with three axles (a front steering axle and two rear tandem axles). The truck designated as "Empty" had no stone placed in the load bed. The truck labeled as "Half" had about half of its load bed filled with stone, whereas the "Full" truck was fully loaded. The weight of the fully-loaded dump truck was the maximum load that the district bridge engineer felt comfortable in loading the structure. Actual axle dimensions and weights are given in Fig. 10. The axle weights were measured by the Virginia Department of Motor Vehicles using enforcement-grade portable truck weigh scales.

LOAD CASES

All three of the dump trucks were positioned in the same orientations for six load cases (LC), shown in Fig. 10. Note that LC 1 and LC 2 are symmetrical to LC 3 and LC 4 with respect to the centerline of the bridge. The purpose for the loading symmetry was to test beams and joints that appeared to be in relatively poor condition (LC 3 and LC 4) with those that were in better condition (LC 1 and LC 2). The trucks for LC 1 and LC 3 were positioned such that one wheel line was centered over the longitudinal joint between the exterior and first interior beams. On the other hand, LC 2 and LC 4 had one wheel line centered over the first interior beam. The purpose of positioning the truck over the longitudinal joint was to impart the most tension across the width of the bottom of the joint, whereas the reason for centering the wheel line over the first interior beam was to assess the joint's ability to transfer load to the exterior beam. The remaining two load cases were designed to assess the strength of Beam 4, where again, Beam 4 was the beam that had exposed and corroded prestressing strands with section loss. Thus, LC 5 had one wheel line centered over Beam 3 (with the overall truck centered over Beam 4), while LC 6 had a wheel line centered over Beam 4 (with the truck centered over Beam 5).

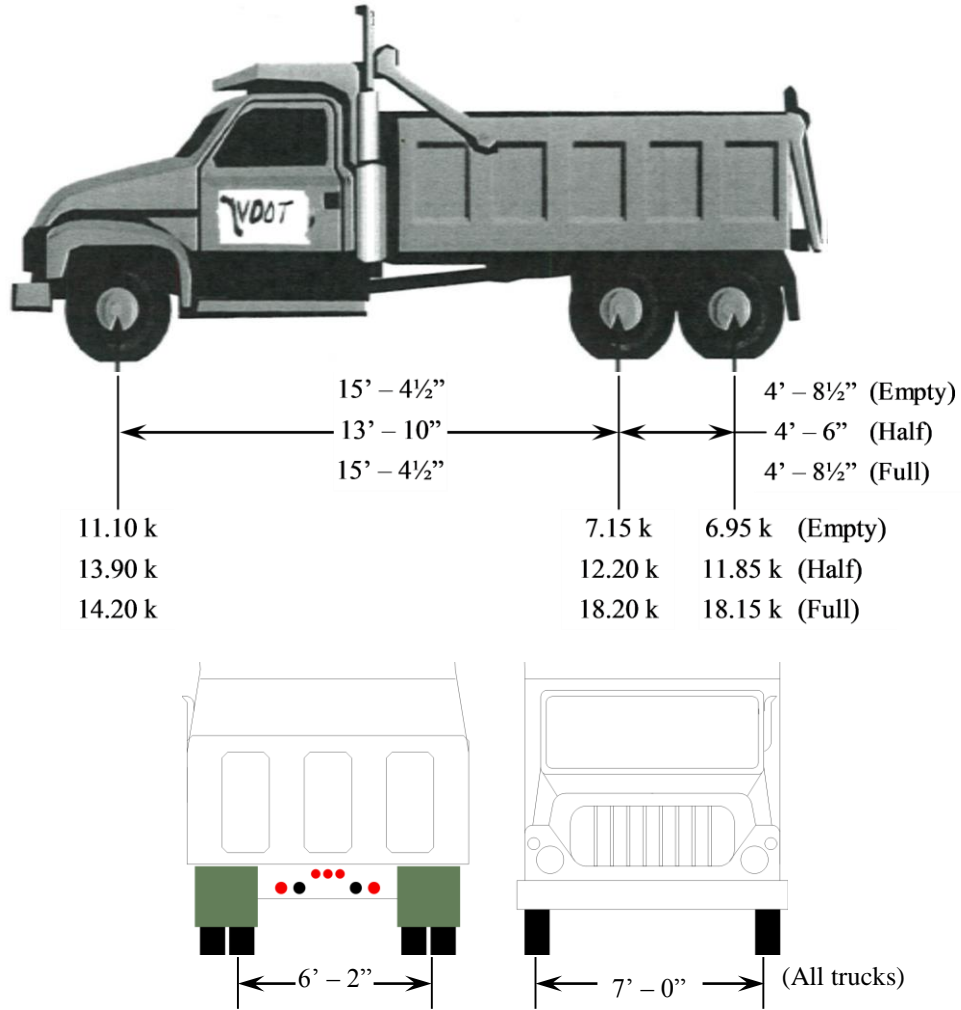


Fig. 10 Dimensions and weights of truck axles used for load test.

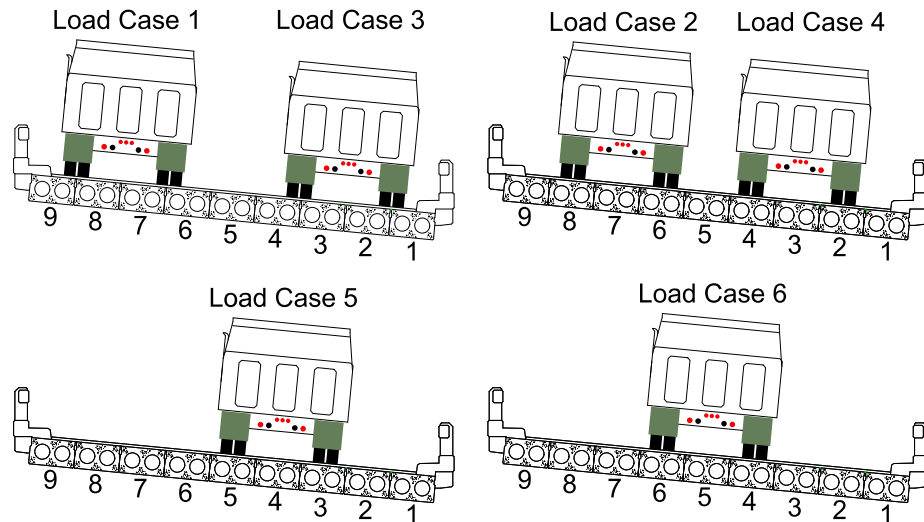


Fig. 9 Various orientations of the load vehicle for the live load testing

TESTING PROCEDURE

There was only one load truck on the bridge during any given test. Due to the geometry of the bridge and the traffic barricades placed at both ends, all tests were conducted with the truck traveling at quasi-static speed, that is, about 2 mph. Each test started with the dump truck parked on Span 2, and was completed once the vehicle was completely off of Span 3 and on Span 4. Unfortunately, there was not enough time to conduct each combination of truck weight and orientation through three repetitions, as desired. However, each test was conducted a minimum of two times, with additional runs conducted as feasible.

RESULTS AND DISCUSSION

MID-SPAN STRAINS IN THE VOIDED SLABS

Fig. 11 shows a typical plot for both the strain at mid-span during a given run of a load truck across Span 3. The peaks in Fig. 11 give an approximate indication of when the three axles were at mid-span. In the particular case of this example, Beam 3, denoted *B3.ms*, had the highest live load strain throughout the test run and was directly underneath the passenger-side wheel line of the load truck. This observation is typical for all of the tests, where the beam underneath the passenger side wheel had the largest recorded strain; the wheel loads on the passenger side of the truck tended to be heavier than on the driver side. A correlating explanation could be that the load vehicles had spring-type suspension that caused more of the load to shift to the passenger side of the vehicle due to the cross-slope going downward on the upstream side of the bridge. However, this possibility could not be confirmed because all load trucks traveled in the same direction for all test runs due to the difficulty in turning the vehicles around.

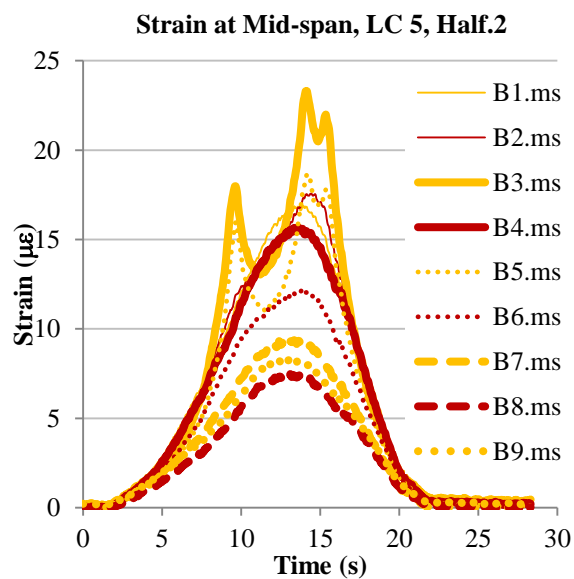


Fig. 11 Typical plot for mid-span strain during live load test

While Fig. 11 details a typical strain plot as a specific load truck traversed Span 3 during a single run for a particular load case, Subplot (a) in Figures 12 through 17 show the relationship between the vehicle weight and the average peak strain responses, respectively, in the individual members for Load Cases 1 through 6. On the other hand, part (b) in Figures 12 through 17 shows the average value of strain for each specific beam at the time the absolute maximum strain amongst all nine beams was recorded during a given test run for a given load case / load truck combination. This comparison shows the relative strain distribution amongst the beams, and will be discussed in the Load Distribution Factors section.

The largest average maximum strain recorded during the entire testing was $40 \mu\epsilon$, which was for Beam 1 in LC 3 using the Full truck. If one were to assume a compressive strength of 4 ksi and a unit weight of concrete of 0.145 kcf in Eq. 5.4.2.4-1 of the 2012 *AASHTO LRFD Bridge Design Specifications*² for calculating the concrete’s elastic modulus, this level of strain would equate to 0.15 ksi of tension in the bottom of the beam due to live load. If assuming simple supports, a girder distribution factor that was slightly larger than the AASHTO-calculated factor (as discussed later in this paper), and a larger moment of inertia for the exterior beam compared to an interior beam (also discussed later in this paper), the theoretical stress due to live load for the given load truck would have been 0.26 ksi. One reason for the discrepancy between theoretical and tested results is that the ends of Beam 1 were not truly simply supported, but had some rotational stiffness that helped to strengthen the beam at mid-span. Nevertheless, if one were to take the prestress losses of $26 \frac{3}{8}$ -in.

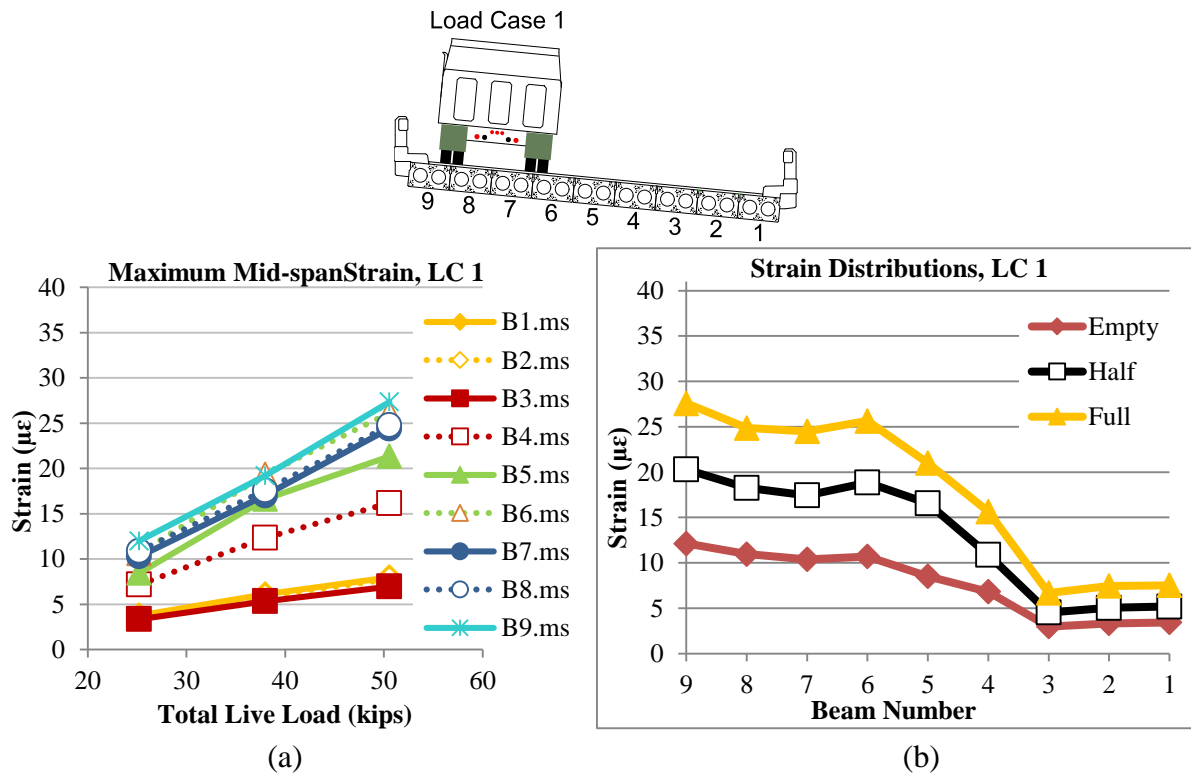


Fig. 12 Average (a) maximum strain and (b) strain distributions at mid-span for all beams [at maximum strain] for Load Case 1.

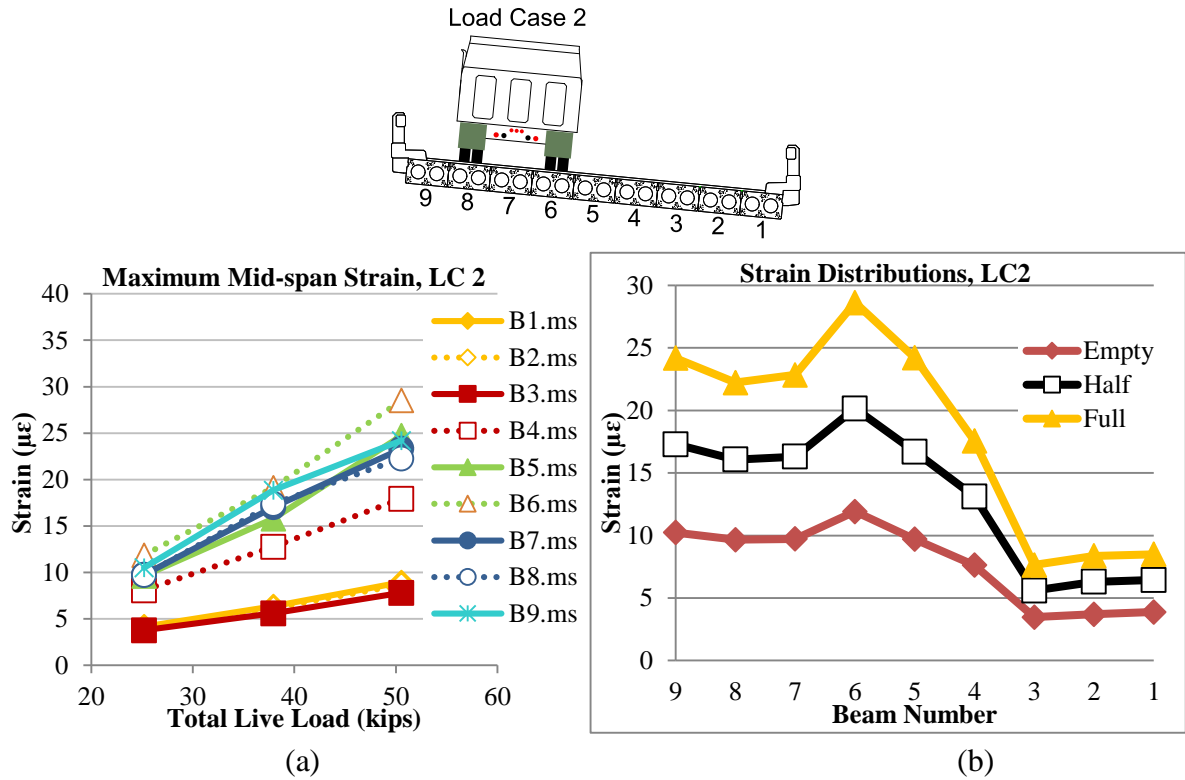


Fig. 13 Average (a) maximum strain and (b) strain distributions at mid-span for all beams [at maximum strain] for Load Case 2.

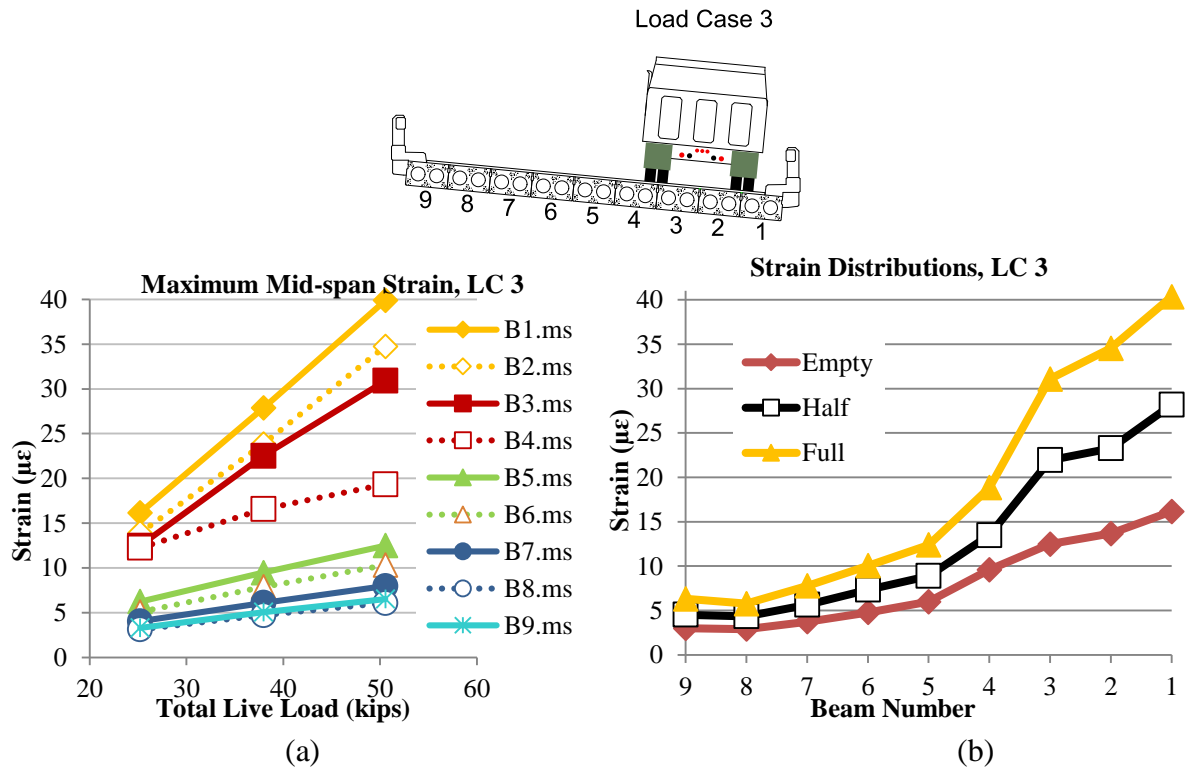


Fig. 14 Average (a) maximum strain and (b) strain distributions at mid-span for all beams [at maximum strain] for Load Case 3.

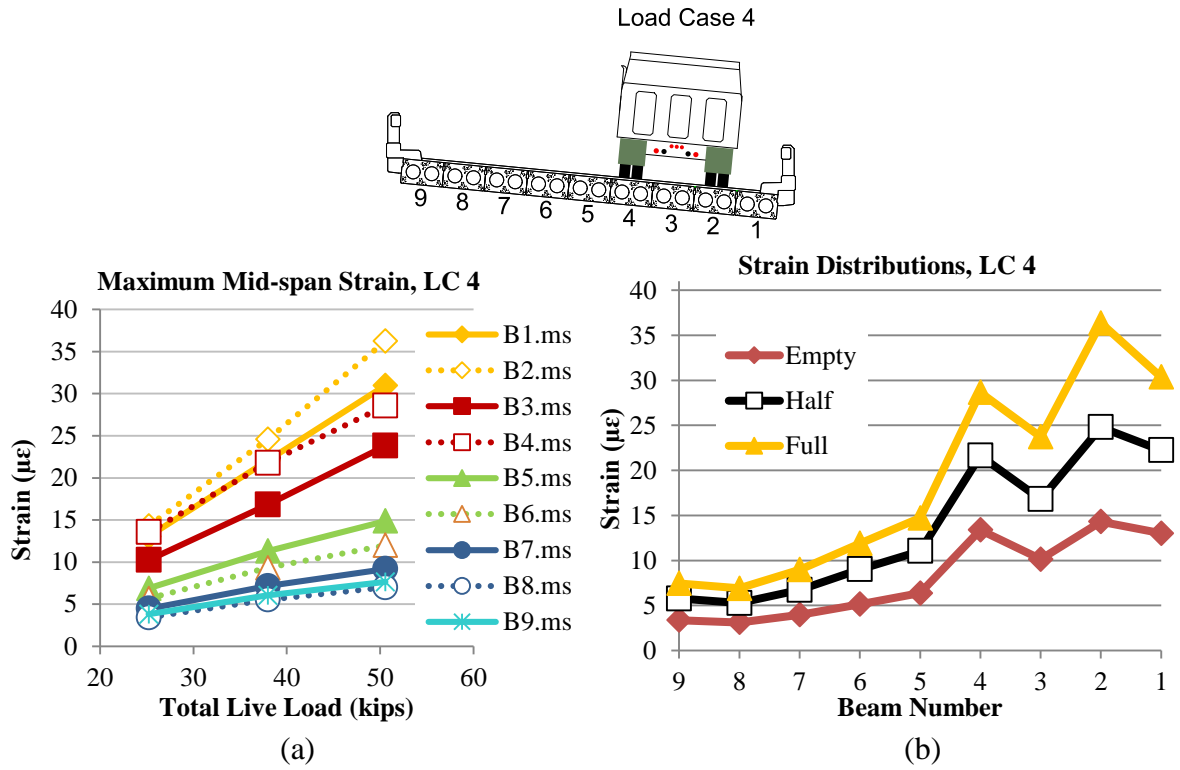


Fig. 15 Average (a) maximum strain and (b) strain distributions at mid-span for all beams [at maximum strain] for Load Case 4.

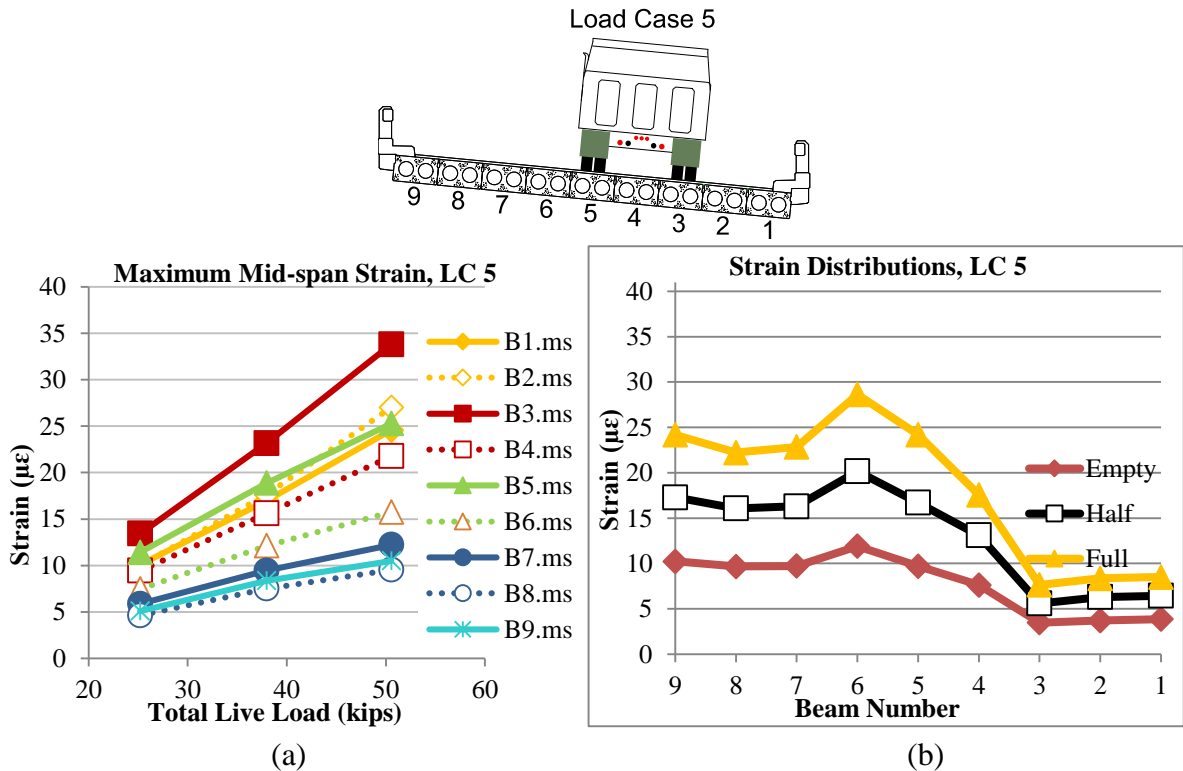


Fig. 16 Average (a) maximum strain and (b) strain distributions at mid-span for all beams [at maximum strain] for Load Case 5.

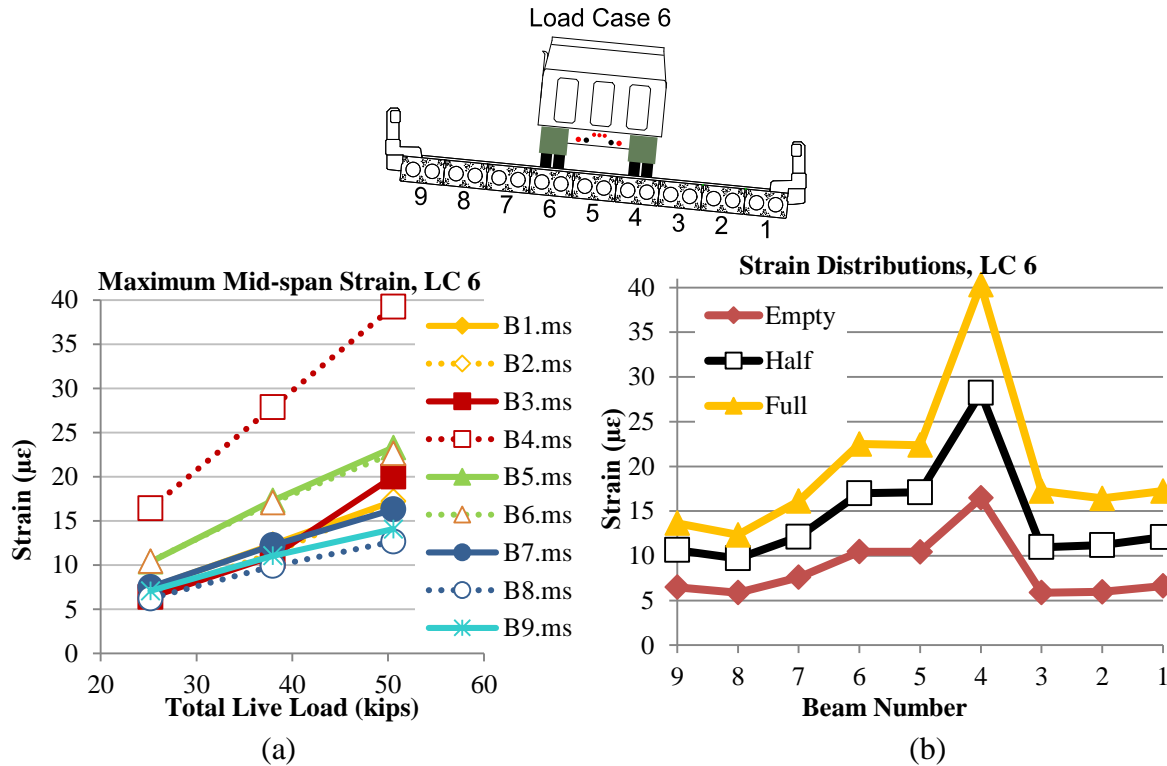


Fig. 17 Average (a) maximum strain and (b) strain distributions at mid-span for all beams [at maximum strain] for Load Case 6.

diameter, Gr. 250 stress-relieved strands into account along with the live load stresses as measured in the field, the total stress in the bottom of Beam 1 would have still been in compression, far from any concerns about cracking. The same was true for the interior beams that had smaller strains due to live load but also smaller section moduli. This result is consistent with the strain versus load graphs in subfigure (a) for Figures 12 through 17, where the strains measured at mid-span increased fairly linearly up to the weight of the Full truck. These linear results show that the structure remained within its linear elastic limit up to 25 tons during the load test, which was about 18 tons less than the inventory rating for a single-unit vehicle on this particular bridge, as listed in the 2011 inspection report.

The exceptions to this linearity in load-strain behavior were Beam 5 in LC 2 [Fig. 13(a)] and Beam 3 in LC 6 [Fig. 17(a)], and to a lesser extent, Beam 6 in LC 2 [Fig. 13(a)] and Beam 2 in LC 4 [Fig. 15(a)]. In these cases, the rate of increase in strain between the Half Truck and the Full Truck was greater than the increase going from the Empty Truck to the Half Truck, on a strain per unit load basis. Recall that Beam 5 had the spall with exposed and broken strand. Interestingly, the non-linearity instances with Beams 5 and 3 occurred when a truck wheel line was adjacent to the beam in question, as opposed to being directly on top. However, the deviation from the linear strain increase for Beams 5 and 3 was only about 5 µε, which is negligible. There were some cases where the rate of strain increase was lower as the amount of load increased. These latter instances, however, occurred in beams that were adjacent to the more directly loaded beams. So, these anomalies may be attributed to minor changes in load distribution as the loading increased. Interestingly, Beam 4 appeared to indicate fairly consistent strain linearity as the load increased. This observation suggests that

the broken strands at the quarter point of that beam did not adversely affect the structural performance at mid-span, which was to be expected as the development length for the prestressing strands was calculated to be about 6 ft. Therefore, the larger strains at mid-span of Beam 4 were probably not due to a lower flexural performance compared to the adjacent members.

Another way to view the strain results in Figures 12 through 17 is to compare beams that experienced similar loading conditions, albeit in different load cases. For instance, take the plots in Fig. 18, which compare the average maximum strains for four beams in select load cases that were under similar loading conditions. Note that the difference between subplots (a) and (b) is that (a) shows data when a wheel line was directly on the centerline of the indicated beam as opposed to the having wheel loads straddle the given beam. The measured strains in each comparison were virtually identical, where the largest difference was about 5 $\mu\epsilon$ when the left wheel line was on top of Beam 3 versus Beam 4, again indicating that the corroded strands in Beam 4 did not have a large impact on the strength of the beam. Beam 5 did have the lowest recorded strains in this comparison, even though this member did have the exposed and broken strand near the quarter-span, as previously mentioned. The driver-side wheel line was directly over Beam 5 in LC5, as opposed to the passenger-side wheel line in the other cases.

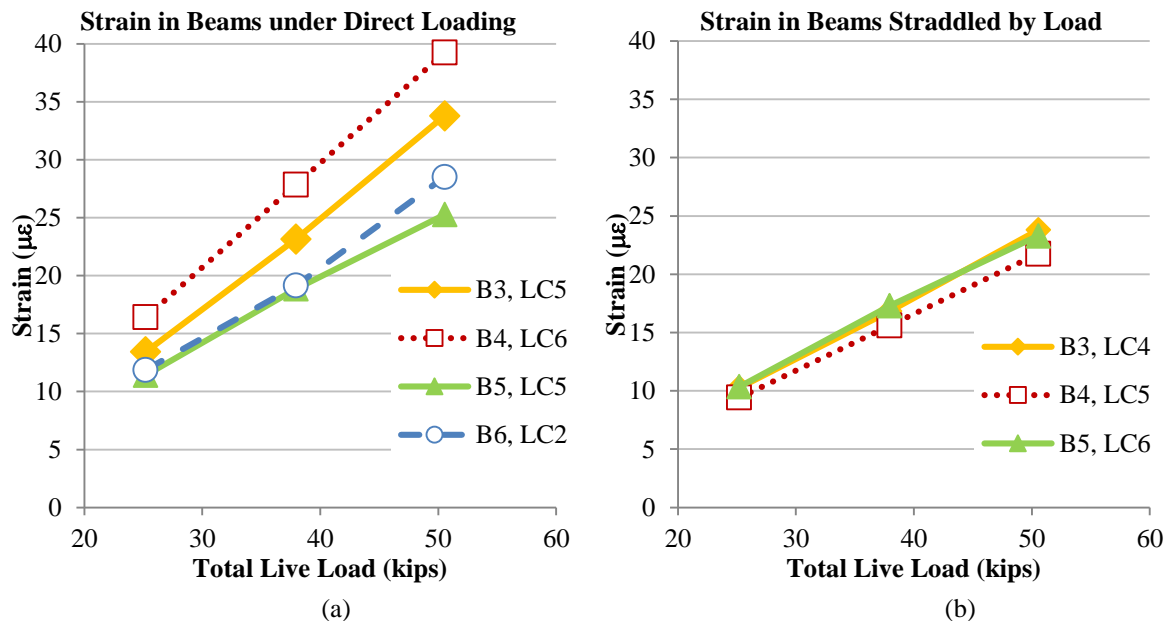


Fig. 18 Given similar loading conditions, a comparison of the strain in (a)

For another comparison, consider the graphs in Fig. 19, which pairs a beam in the southbound lane with one from the northbound lane that was symmetric to the bridge centerline and subjected to a similar load pattern. Note that the beams in this figure are paired together in the legend according to their symmetric location, and plots for the beams in the southbound lane are solid lines whereas the beams in the northbound lane are dotted lines. Furthermore, note that Fig. 19(c) is simply a reconfiguration of the results for Load Case 6 in Fig. 17(a). For the most part, the scenarios in Fig. 19 demonstrate that the peak strains in the

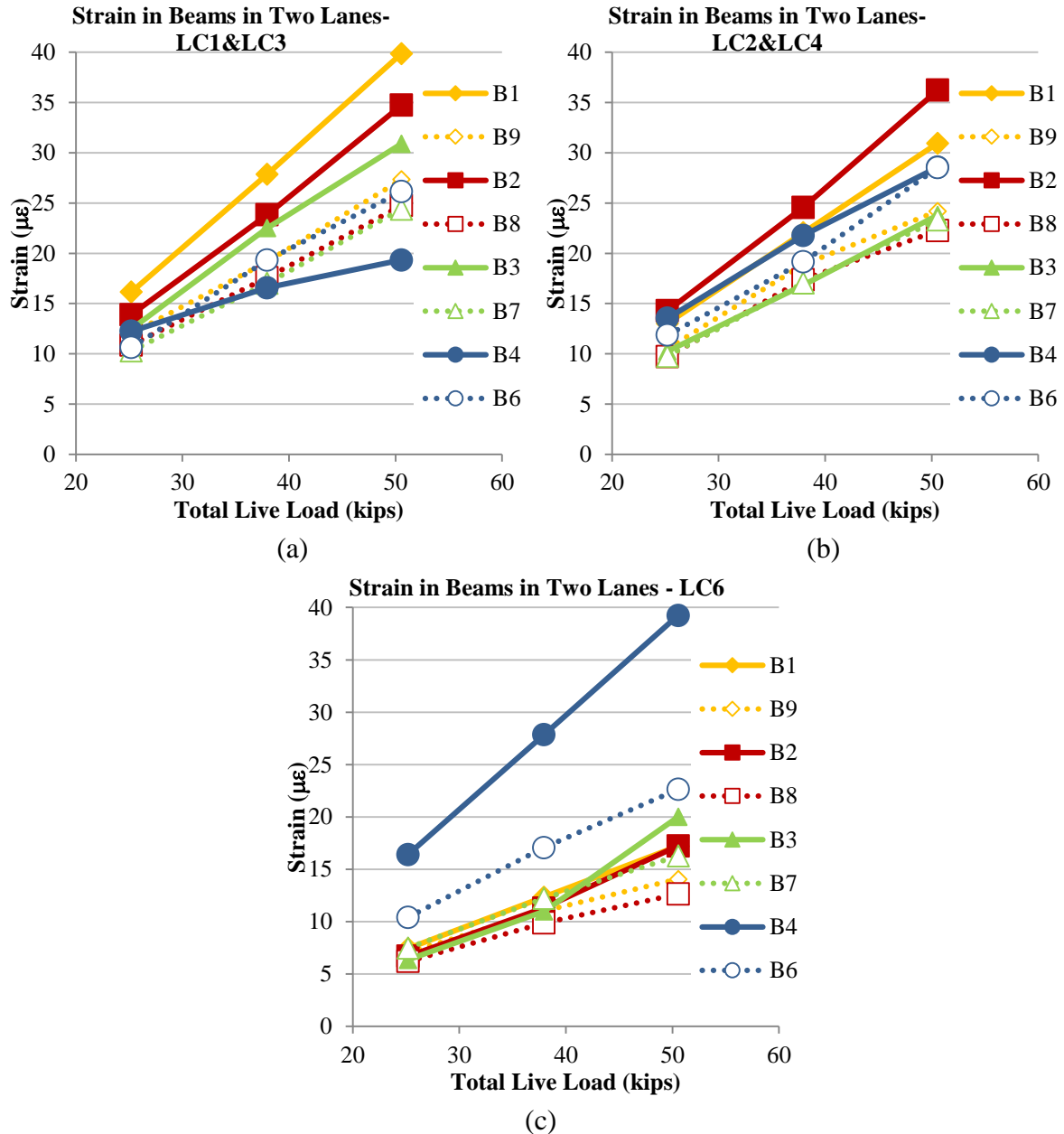


Fig. 19. Comparison of strains in beams symmetric to the bridge centerline for (a) Load Cases 1 and 3, (b) Load Cases 2 and 4, and (c) Load Case 6.

beams in the southbound lane were generally slightly greater than those in the northbound lane. Note that the southbound lane is the lane on the lower end of the super-elevation. Thus, the southbound lane was likely the side of the bridge where snow would pile up during snow removal, and certainly the side subjected to more chloride during snow melts and rain run-off. Thus, the beams in the southbound lane could conceivably have had a greater degree of deterioration, and thus be the reason why that lane exhibited larger strains during the load test.

With that said, one fact that should be highlighted is that the differences in strain between the two travel lanes were fairly minute. For added emphasis, recall that the strain results from testing indicated that the bottoms of the prestressed concrete voided slabs were in compression even under the heaviest loading condition. Granted, the maximum test load was only 58% of the inventory rating from the previous inspection report, and the testing did not include dynamic effects due to situational limitations. However, the information gained from the load test could be used to model or estimate the safe load capacity of the structure and compare that result with the previous rating.

LOAD DISTRIBUTION FACTORS, g

Regarding the load distribution graphs seen in subfigure (b) of Figures 12 through 17, if the load were evenly spread out across all of the beams in a bridge, then the amount of strain in each beam would be identical. However, if the weight of a truck is solely borne by the beams directly underneath the truck's wheels, then a more localized distribution of the load would be indicated by a sizable change in the strain in those beams relative to the other members. While all of the load cases during this test had distribution results that were somewhere in between these two outcomes, Load Case 1 was closer to the former scenario, where Beams 5 through 9 had a relatively similar amount of strain (at the time of maximum strain) when the truck was located on the elevated half of the bridge.

On the other hand, the remaining load cases do show a little bit of a spike in the load distribution graphs. This spike is most evident in LC 6, where the maximum strain was 60% (for the Empty load truck) to 80% (for the Full load truck) greater than the largest strain in an adjacent beam. For LC 6, one of the wheel paths of the load truck was directly over Beam 4. Given that similar, albeit less prominent, changes in strain levels occur in Load Cases 3 through 5, where a wheel path is over or adjacent to Beam 4, the data indicate that the longitudinal joints on either side of Beam 4 are no longer intact. Although the researchers observed that there was virtually no efflorescence at these two joints, the damage to the joints may have been relatively recent such that mineral buildup did not have sufficient time to develop. Regardless, there is at least some degree of load distribution occurring in each of the six load cases, as indicated by the amount of strain in all of the beams, with the exception of those members farthest away from the load truck.

The data in each subplot (b) of Figures 12 through 17 can be condensed to a single value, known as the load distribution factor, g . This factor is the fraction of the vehicular load that is directly applied to any one beam, expressed as the ratio of the maximum strain found amongst all of the beams, divided by the sum of the strains in all of the beams at the time that the maximum strain was recorded. The greater the value of g , then the lesser the amount of load that is being distributed to the beams adjacent to the beam that is directly underneath the wheel line of the vehicle.

The average distribution factors for moment for each of the six different load cases are tabulated in Table 2. The largest average factor was 0.24 for LC 3, based on a total of six runs for three different load trucks. In comparison, Table 4.6.2.2.2b-1 of the *2012 AASHTO LRFD Bridge Design Specifications*² provides formulas for calculating the design live load moment distribution factors for bridges constructed of precast voided boxes with shear keys,

Table 2. Moment load distribution factors based on strain measurements from the various load cases.

Load Case	Distribution Factor	
	Average	CoV
1	0.17	0.02
2	0.17	0.01
3	0.24	0.03
4	0.20	0.04
5	0.18	0.04
6	0.22	0.00

but with no cast-in-place deck overlay, that is the typical cross-section “g” in Table 4.6.2.2.1-1 of the *Specifications*. The calculated values for g are given in Table 3. Note there are two different possible calculations depending on whether there is sufficient transverse post-tensioning to cause the individual box sections to act as a complete unit or the post-tensioning that is provided only inhibits vertical displacement at the beam interface. Also, the distribution factor calculation depends on whether the beam is an exterior beam or an interior member. Regardless, all of the results in Table 3 assume one design lane is loaded, as there was only a single truck on the bridge during testing. These calculations also assume that the curvature of the structure in plan is relatively small (less than 12 degrees, according to Article 4.6.2.2.1 and Article 4.6.1.2.3 [AASHTO 2012]). As mentioned earlier, the Adkins Road bridge has a central angle of 7° , so the curvature of the structure should not contribute to the live load distribution effects.

Table 3. Distribution factors calculated according to AASHTO

P/T condition	g	
	Interior	Exterior
beams act as complete unit	0.21	0.23
no vertical displacement at interface	0.26	0.28

As the largest experimental value for g found from six different load cases, 0.24 could be considered the distribution factor for the entire bridge. However, the load case that generated the maximum distribution factor, LC 3, had a wheel line being supported by both an exterior and an interior girder. Thus, determining whether the interior beam or exterior beam was the controlling element in this load test is difficult to do. Furthermore, none of the various truck orientations included a wheel line directly over either of the exterior beams due to the curb at the edge of the bridge deck. Therefore, comparing the calculated g for the exterior girders with the physical load test is not possible. Nonetheless, one can consider the results in Table 2 for Load Case 2 and Load Cases 4 through 6, where only interior girders were loaded and the wheel line was directly above a single beam versus on a joint between two members. For these three cases, g ranged from 0.17 to 0.22. Given that these values are closer to 0.21 than 0.26 from Table 3, the conclusion is that the individual interior beams were acting as a single unit. Note that a value of 0.24 for LC 3 from Table 2 was used to calculate the moment

applied to Beam 1 during the load test, as discussed in the section, *Mid-span Strains in the Voided Slabs*.

STRAINS AT THE QUARTER-SPANS

Unfortunately, one of the BDI STS Wi-Fi nodes that was connected to three sensors was not properly configured; hence, no data was collected from either the two strain gauges located at the quarter-point closest to Bent 2 for Beams 3 and 4, or the tiltmeter adjacent to Bent 2. Thus, no comparisons can be made with the symmetrically located sensors closer to Bent 3. Furthermore, no analysis could be done for the hole discovered at the quarter-span closest to Bent 2 in Beam 5. Nevertheless, Table 4 compares the average maximum strain at the measured quarter-points in Beams 3 and 4 along with the average maximum strain at mid-span, with the passenger-side wheel line directly over the respective beam in LC 5 and LC 6. Again, Beam 4 was the voided slab that had the exposed and corroded strands near the quarter-point in question; these strands likely contributed little resistance to flexural strain at that location. Thus, the strain at the bottom of Beam 4 at the quarter-point should have been greater compared to Beam 3. However, the data show that Beam 4 had noticeably lower strains at that location relative to Beam 3. On the other hand, Table 4 also lists the average maximum strain at mid-span and quarter-span for Beam 3 during LC 6, which again is the load case where the wheel line was directly on top of Beam 4. Despite having lower average strains at mid-span relative to Beam 4 for the same truck orientation, Beam 3 had larger strains at the quarter-span. Perhaps delaminations near the spalled section in Beam 4 were not visibly apparent such that debonding along the strand-concrete interface or internal cracking in the concrete prevented stresses from transferring through the material to the strain sensor at that the quarter-point for Beam 4. Another possibility is that poor consolidation of the concrete at the location, as seen in Fig. 7, also affected the results. If there was improper consolidation, then there may have been insufficient transfer length needed to transmit the stress from the strands to the concrete.

Table 4. Average Maximum Strain Comparison Between Mid-Span and a Quarter-Point for Beams 3 and 4, Loaded with a Full Truck.

Load Case	Beam	Truck	Strain ($\mu\epsilon$)	
			Mid-span	Quarter-span
5	3	Empty	13	10
		Half	23	14
		Full	34	20
6	4	Empty	16	2
		Half	28	4
		Full	39	5
6	3	Empty	6	6
		Half	11	8
		Full	20	15

STRAINS IN THE PARAPETS

Refer back to Figures 12 and 14, where a wheel line from the load truck was positioned on top of the longitudinal joint between the fascia beam and the first interior beam. These two orientations are the most direct loading on the fascia beams during the entire load test. In both cases, note how the strains were greater in the exterior beams than the interior beam. These larger strains are indicative of the fact that the exterior beams did not benefit from having adjacent members on both sides of the given beam in distributing the load in the same manner as the interior beams. However, the exterior beams did have a parapet, which could have increased the stiffness of those exterior members. In the case of the Adkins Road bridge, the railing and curb were continuous along the length of the span. The question is whether or not there was substantial composite action occurring between the beam and the parapet to further augment the beam stiffness.

Table 5 summarizes the average strain due to live load at mid-span of the bottom of Beam 1, *Bl.ms*, along with the average strain occurring near the bottom and top of the parapet, *Bl.pB* and *Bl.pT*, respectively, at the time that the strain in the bottom of the slab reached its maximum. Positive values in the table indicate that the live load had a tensile effect, whereas negative values meant a compressive effect. Note that the values in the table are for LC 3, where the wheel line was closest in proximity to the centerline of Beam 1; thus, the strains in this table are the largest strains observed in Beam 1 throughout the live load tests.

Table 5. Average Maximum (or Minimum) Strains at Mid-Span of the Upstream Fascia Beam for LC 3.

Truck	Strain ($\mu\epsilon$)		
	beam _{bottom} (<i>Bl.ms</i>)	curb (<i>Bl.pB</i>)	railing (<i>Bl.pT</i>)
Empty	16	-9	-9
Half	28	-15	-14
Full	40	-20	-18

In examining whether or not the parapet acted compositely with the beam, consider Fig. 20, which shows a cross-section of Beam 1 along with the parapet attached to the beam. Note that portions of the parapet are not colored in because those sub-elements were not continuous along the entire span length. Although the curb element was not connected to the beam along the entire span due to the scuppers that were designed to allow water drainage, the curb was positively attached to the fascia beam at the location of the railing posts, which were spaced at 9 ft - 7. ¼ in. Also indicated in the figure are the locations of the strain gauges and the average maximum strains recorded due to a fully loaded dump truck in the LC 3 position. The other strain values in the figure were calculated assuming three different levels of composite action: the beam, curb, and top railing being fully composite; only the beam and curb acting compositely; and no composite action at all.

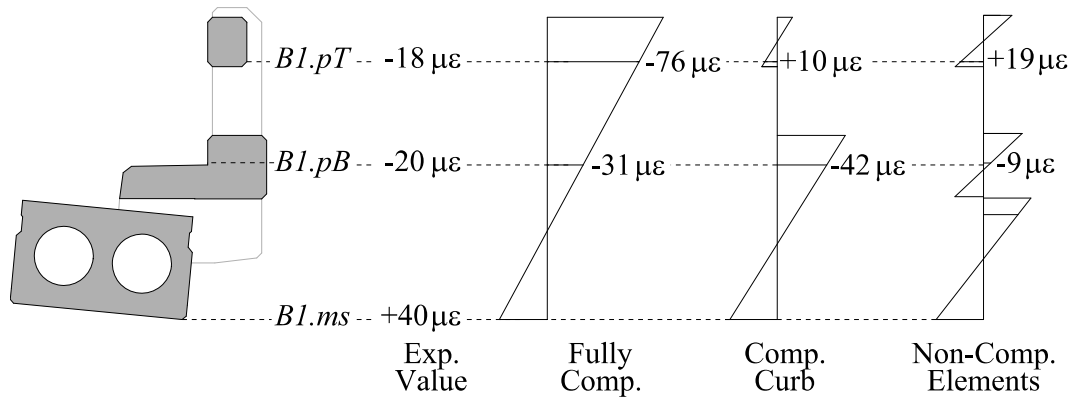


Fig. 20. Comparison of experimentally-measured strains versus calculated values assuming various degrees of composite action

The compressive strength of the concrete in the beam was assumed to be 4 ksi while the strength of the curb and railing was assumed to be 2.5 ksi. The section properties of the curb and railing were transformed to that of the beam using calculated values for the modulus of elasticity. The moment applied to the non-composite sections was taken as a percentage of the calculated moment in the composite section for a given scenario, where the percentage was the ratio of the transformed moment of inertia of the non-composite element versus the moment of inertia of the composite section. The moment applied to the composite section was calculated using the measured strain in the bottom of the beam and the equation

$$M_c = \frac{\varepsilon_{Bl.ms} E_{beam} I_c}{y_{bot}}$$

where:

$\varepsilon_{Bl.ms}$ = maximum measured strain in the bottom of Beam 1 when the fully-loaded truck was oriented with a wheel line over the longitudinal joint between Beams 1 and 2.

E_{beam} = calculated modulus of elasticity of the voided slab

I_c = moment of inertia of the composite section

y_{bot} = distance from the centroid of the composite section to the bottom fiber of the composite section

Varying the assumed compressive strength, and hence the elastic modulus, did not have a major impact on the calculated strain values given in Fig. 20. In any event, comparing the experimentally recorded strains versus the calculated values revealed a slight amount of composite action occurring between the exterior beam and the parapet components. If, in fact, the railing was truly non-composite, then the railing would not feel any realistic load from the truck. However, the railing could have had additional deflection under self-weight when the supporting beam beneath the railing deflected downward and away from the railing due to the weight of the truck, and thus, the bottom of the railing would exhibit a small amount of tension. Instead, the load test showed that the bottom of the railing exhibited a small amount of compressive strain. On the other hand, the strain gage on the curb had less compressive strain than for either scenario that assumed composite action with the beam but had more compressive strain than what was calculated for the non-composite curb element. One possible explanation as to why the railing appeared to have a greater degree of

composite action compared to the curb is that the strain gage was not adequately attached to the concrete at the top of the curb due to the surface conditions of the curb. Thus, perhaps the recorded strain in the curb did not fully account for the actual strain in that element.

DIFFERENTIAL DISPLACEMENTS BETWEEN BEAMS

Fig. 21 shows a comparison in the typical behavior of two different longitudinal joints at mid-span of Span 3, where Joint 1 was considered to be a representative joint in poor condition whereas Joint 7 was similar to other joints deemed to be in relatively good condition, based on visual observation of the underside of the bridge. Note that this figure considers a fully-loaded dump truck for two separate load cases, LC 4 and LC 2, for the two respective joints. These two load cases are the only comparable truck orientations where a wheel line from the load vehicle was adjacent to a longitudinal joint at which differential displacement was measured. While the truck orientations themselves were symmetrical with respect to the centerline of the bridge, the two joints did not receive quite the same loads. The difference lies in the fact that Joint 1 was primarily loaded with the passenger side of the dump truck while the driver side of the vehicle was adjacent to Joint 7. Again, because of the nature of the weight distribution of the truck, Joint 1 experienced about 2% greater load than Joint 7.

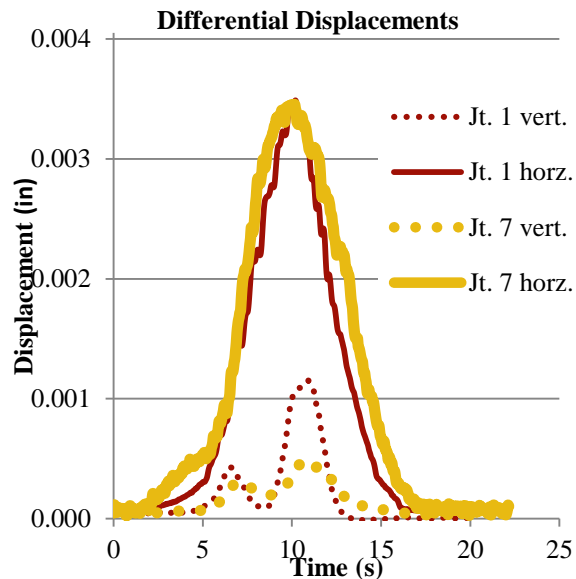


Fig. 21 Comparison of differential displacements at mid-span for Joints 1 and 7

Fig. 21 indicates that the LVDTs at mid-span of Joints 1 and 7 were able to detect responses to the load vehicle as it traversed the span. However, the relative displacements at both joints were both extremely small, with the largest vertical differential movement being just above 0.001 in. Interestingly, the differential horizontal displacement was greater than the vertical displacement in both joints. Even so, the recorded displacements were below the precision in the LVDT devices, which was 0.005 in. Nevertheless, just as a point of comparison, the two longitudinal joints had a similar degree of horizontal movement between the two beams at the given joint. On the other hand, Joint 1 had about twice as much vertical differential

movement as did Joint 7. Again, however, greater emphasis should be placed on the fact that all of the measured movements between two beams were fairly minute.

Looking solely at Joint 1, Fig. 22 is a typical comparison of the movement between Beams 1 and 2 under two different load scenarios. Fig. 22(a) looks at the behavior when a wheel line from the load truck was positioned directly over the joint, whereas Fig. 22(b) is the result of having a wheel line centered on a beam adjacent to the joint. The measurements in these plots are quite small, with the differential vertical displacement being less than the horizontal movement. As expected, the movement between Beams 1 and 2 in the horizontal direction tended to be less when the wheel load was located adjacent to the longitudinal joint (that is, LC 4) compared to when the wheel load was directly over the joint, as in LC 3. Furthermore, the differential horizontal movement at mid-span was slightly greater than at the two quarter-points. On the other hand, the vertical differential displacement was marginally greater for LC 4.

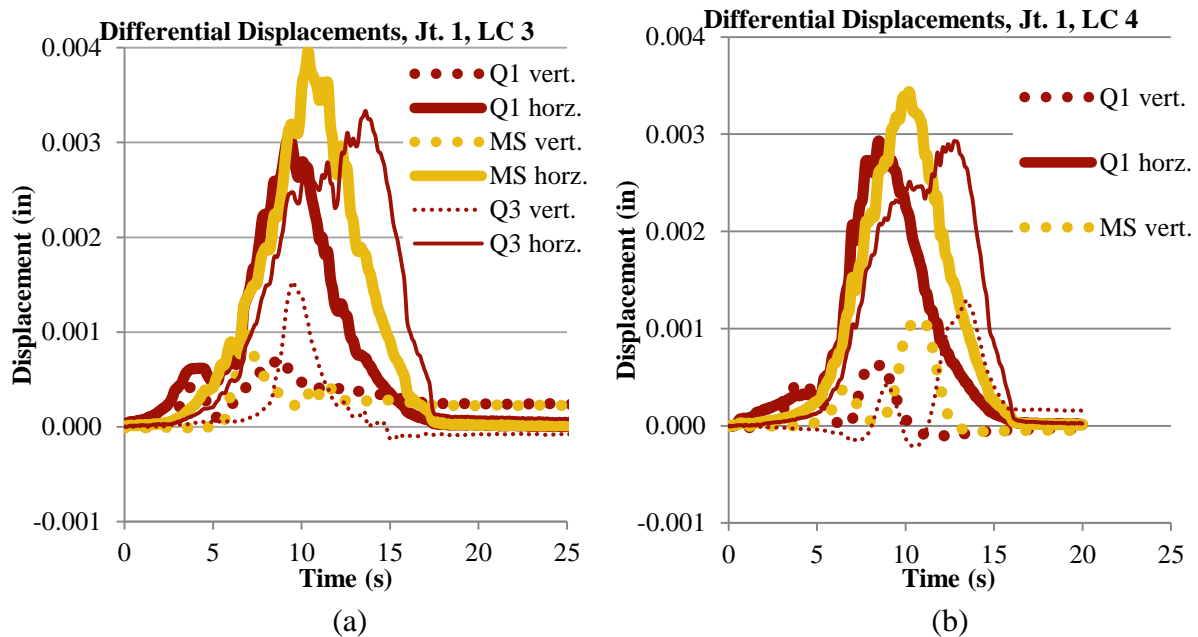


Fig. 22 Differential displacements between Beams 1 and 2 for (a) Load Case 3 and (b) Load Case 4.

BEAM ROTATIONS

As stated earlier, the intent had been to compare the rotations at both ends of Beam 4. However, the data collection system was not properly configured to receive information from the tiltmeter located at the end of Beam 4 at Bent 2. Thus, no comparison can be made between the two ends of the beam. Nevertheless, the rotation at the one end of the beam appeared to be fairly small, as shown in Table 6. Even for the most heavily loaded vehicle, the rotation of the beam end had an average maximum value of about 0.7 degrees, which was about the same as the theoretical rotation based on simple hand calculations for simply-supported members. Additionally, Load Cases 3 through 6 essentially had the same degree of rotation for the respective loads. These recorded rotations were fairly low, even when compared to previous experience with adjacent, prestressed concrete members.

Table 6. Average maximum measured rotations, in degrees, for Beam 4 near Bent 3.

Truck	Load Case			
	3	4	5	6
Empty	0.4	0.4	0.3	0.4
Half	0.5	0.5	0.5	0.5
Full	0.7	0.7	0.7	0.7

CONCLUSIONS

Based on the results of the live load testing, the authors have made the following conclusions about the adjacent, prestressed concrete voided slab elements in the Adkins Road bridge:

- Reflective longitudinal cracks that had formed through the asphalt riding surface, thus allowing chloride-laden water to drain through the joints and down to the bottom of the beams only had a minor impact on the structural performance of the bridge. Although the beams on the downslope (upstream) side did have slightly larger mid-span strains compared to those beams on the upslope (downstream) side of the bridge, the differences were relatively minute. While the actual condition of the post-tensioning reinforcement could not be assessed, if the ties were indeed functioning as designed, then the effect would be improved lateral transfer of the load compared to if there was no transverse force being applied.
- Despite signs of deterioration in the longitudinal joints, as suggested by the efflorescence that had formed along the joints at the bottom of the beams, the grouted shear keys in those joints appeared to still be performing well. There were virtually no vertical or horizontal differential displacements at the two joints that were monitored during the load test to the point where all recorded measurements were less than the precision of the measurement instruments. One joint was deemed to be a good joint without efflorescence while the other joint was in a more dilapidated state that had efflorescence.
- The exterior girders did benefit from additional stiffness provided by the barriers, which exhibited at least some degree of composite action with the fascia beams.
- The exposed and corroded or broken strands in Beams 4 and 5 appeared to have a relatively negligible impact on the beams' flexural performance when compared to adjacent beams subjected to similar loading conditions.
- The beams in the structure were still within their elastic limit during the load test, as supported by the fact that the strain versus load plots in Figures 12 through 17 were generally linear. Furthermore, the analysis showed that the bottom fiber of the beams were still in compression when loaded with a 25-ton, 3-axle dump truck and assuming certain material properties of the concrete and force in the prestressing strands. Therefore, the Adkins Road Bridge still retained adequate flexural strength to support service loads.

- After 54 years of service, there was still some degree of load distribution across these longitudinal joints. The AASHTO LRFD-calculated girder distribution factors for moment were slightly conservative compared to the experimentally-derived factors, although it was not possible to directly calculate g for an exterior beam. When considering those load cases where only interior beams were loaded with wheel loads centered on the centerline of a beam, g was less than or close to the AASHTO LRFD-calculated values assuming all of the beams acted as a complete unit. Nevertheless, for the sake of conservancy, the authors support the current method for calculating the distribution factors for moment loads in adjacent, prestressed concrete voided slabs.

ACKNOWLEDGMENTS

The authors would like to thank Dr. Richard Weyers, who was helpful in assessing the condition of the bridge prior to the load testing. Additionally, John Civitillo, Daniel Hailesalassie, and Chad Anderson were pivotal in instrumenting the structure. Lastly, thanks to Gary Martin, Robert Dunn, and Brad Jones of VDOT's Richmond District for their cooperation and coordination of access underneath the bridge and the load trucks used for the test.

REFERENCES

1. Virginia Department of Transportation, *Manual of the Structure and Bridge Division, Vol. 2: Design Aids and Typical Details*, VDOT, Richmond, 2014, p. 12.08-1.
2. AASHTO, *AASHTO LRFD Bridge Design Specifications*, 6th ed., American Association of State Highway and Transportation Officials, Washington, D.C., 2012.